Physics of the Earth and Planetary Interiors 253 (2016) 21–30

Contents lists available at ScienceDirect

Physics of the Earth and Planetary Interiors

journal homepage: www.elsevier.com/locate/pepi

Strong seismic scatterers near the core–mantle boundary north of the Pacific Anomaly

Xiaolong Ma [a,b], Xinlei Sun [a,c,*], Douglas A. Wiens [c], Lianxing Wen [d,e], Andrew Nyblade [f], Sridhar Anandakrishnan [f], Rick Aster [g], Audrey Huerta [h], Terry Wilson [i]

[a] State Key Laboratory of Isotope Geochemistry, Guangzhou Institute of Geochemistry, Chinese Academy of Sciences, Guangzhou 510640, China
[b] Universtiy of Chinese Academy of Sciences, Beijing 10069, China
[c] Department of Earth and Planetary Sciences, Washington University (St. Louis), United States
[d] Department of Geosciences, State University of New York at Stony Brook, United States
[e] Department of Earth and Space Sciences, University of Science and Technology of China, China
[f] Department of Geosciences, Pennsylvania State University, United States
[g] Department of Geosciences, Colorado State University, United States
[h] Department of Geological Sciences, Central Washington University, United States
[i] Department of Geological Sciences, Ohio State University, United States

ARTICLE INFO

Article history:
Received 24 October 2015
Received in revised form 25 January 2016
Accepted 25 January 2016
Available online 2 February 2016

Keywords:
Seismic scatterers
PKP precursor
Subducted slabs
Lateral heterogeneities
Core–mantle boundary

ABSTRACT

Tomographic images have shown that there are clear high-velocity heterogeneities to the north of the Pacific Anomaly near the core–mantle boundary (CMB), but the detailed structure and origin of these heterogeneities are poorly known. In this study, we analyze PKP precursors from earthquakes in the Aleutian Islands and Kamchatka Peninsula recorded by seismic arrays in Antarctica, and find that these heterogeneities extend ~400 km above the CMB and are distributed between 30° and 45°N in latitude. The scatterers show the largest P-wave velocity perturbation of 1.0–1.2% in the center (160–180°E) and ~0.5% to the west and east (140–160°E, 180–200°E). ScS–S differential travel-time residuals reveal similar features. We suggest that these seismic scatterers are the remnants of ancient subducted slab material. The lateral variations may be caused either by different slabs, or by variations in slab composition resulting from their segregation process.

1. Introduction

The core–mantle boundary (CMB) is one of the most significant boundary layers within the Earth. This layer and its adjacent regions, especially D″, are key to understanding dynamic processes within the Earth, such as the source of mantle plumes, the fate of subducted slabs, and material and heat exchange between the mantle and core (Young and Thorne, 1987; Wysession et al., 1994; Lay et al., 1998; Garnero, 2000, 2004; McNamara and Zhong, 2005; Lay and Garnero, 2011). Previous seismological studies have found complex heterogeneities near the CMB, such as Large Low Shear Velocity Provinces (LLSVPs) (e.g., Wen, 2001; Ni and Helmberger, 2003; Wang and Wen, 2007; Garnero and McNamara, 2008; He and Wen, 2009, 2012), Ultra-Low-Velocity zones (ULVZ) (Garnero and Vidale, 1999; Rost et al., 2006; Rost et al., 2010; Yao and Wen, 2014), anisotropy (e.g., Kendall and Silver, 1996; Lay et al., 1998; Garnero et al., 2004; Long, 2009), and seismic scatterers (e.g., Cleary and Haddon, 1972; Husebye and King, 1976; Vidale and Hedlin, 1998; Thomas et al., 1999; Hedlin and Shearer, 2000; Cao and Romanowicz, 2007; Vanacore et al., 2010). Although high-velocity anomaly regions are well studied and are commonly attributed to subducted slabs, many regions, because of inadequate sampling by conventional seismic phases, are poorly imaged. In addition, conventional tomographic methods often poorly resolve small-scale structures due to limited frequency content. In this case, unconventional methods, such as those specifically focusing on scattered waves, may provide additional information. For the lowermost mantle, PKP precursors are possible candidates to serve this purpose.

PKP precursors are P waves that are scattered by small-scale elastic heterogeneities in the mantle and/or topographic irregularities on the CMB (e.g., Cleary and Haddon, 1972; Haddon and Cleary, 1974; Doornbos, 1976, 1978; Bataille and Flatté, 1988; Cormier, 1995; Hedlin and Shearer, 2000). Because of the geometry ray-paths of these seismic phases, the scattered P waves can

* Corresponding author at: State Key Laboratory of Isotope Geochemistry, Guangzhou Institute of Geochemistry, Chinese Academy of Sciences, Guangzhou 510640, China.
E-mail address: xsun@gig.ac.cn (X. Sun).

http://dx.doi.org/10.1016/j.pepi.2016.01.007
0031-9201/

precede the core phase (PKIKP) by up to 20 s and are typically best recorded at a distance range between 120° and 142° (Fig. 1). Particular advantages of using PKP precursors are that they are sensitive to heterogeneity at a scale as small as ~10 km, and are not contaminated by the coda of other phases due to their earlier arrival times. There have been successful applications of PKP precursors studies on global scales (e.g., Hedlin et al., 1997; Cormier, 1999; Margerin and Nolet, 2003b; Mancinelli and Shearer, 2013), as well as regional scales (e.g., Vidale and Hedlin, 1998; Wen and Helmberger, 1998; Niu and Wen, 2001; Miller and Niu, 2008; Thomas et al., 2009; Frost et al., 2013). In regional studies that incorporate well-sited arrays of seismographs, greater information about the anomalies, such as their boundary locations and sharpness, may be resolvable.

In this study, we focus on the CMB region to the north of the Pacific Anomaly, a region where tomographic images consistently show large-scale high-velocity anomalies (Li and Romanowicz, 1996; Grand, 2002; Zhao, 2004; Li et al., 2008; Simmons et al., 2010) but where high resolution details are lacking. We use PKP precursors from earthquakes in the Aleutian Islands and Kamchatka Peninsula recorded by recently deployed seismic arrays in Antarctica to locate the scatterers and to investigate their velocity variations. Our results show that the observed precursors are caused by seismic scatterers in the lowermost mantle, and the strengths of these scatterers vary according to their locations. Furthermore, we also analyze ScS–S travel time residuals sampling the same region, and find that the results show similar variation pattern. We suggest that the lateral variations in this region may be caused by heterogeneities from different subducted slabs, or by varying chemical compositions of the slab resulting from their segregation process.

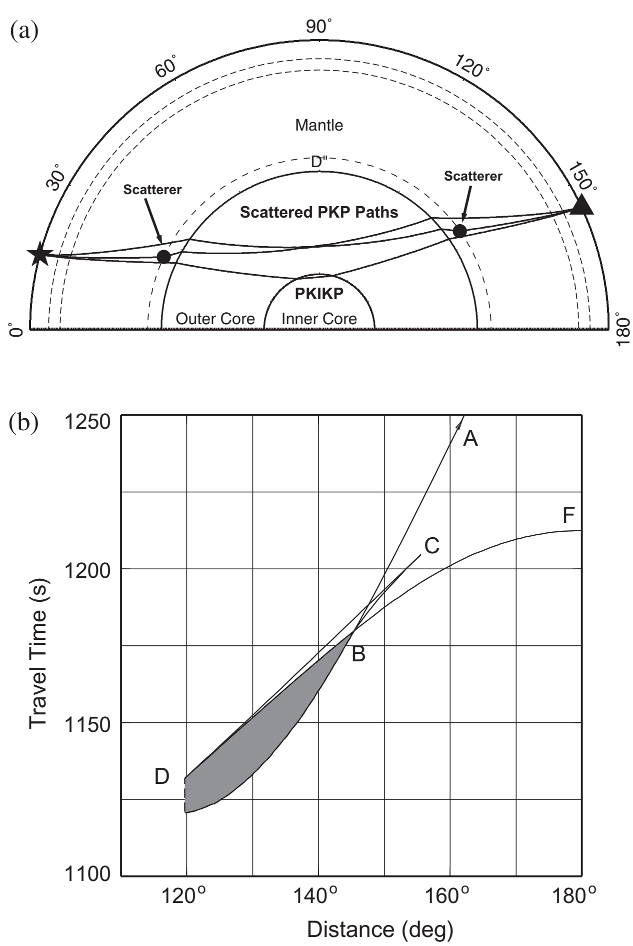

Fig. 1. (a) Ray-paths of PKIKP and scattered PKP waves. The PKP precursors are scattered PKP waves generated by the seismic scatterers (black dots) in the lower mantle beneath the source or receiver. The five-pointed star denotes the earthquake at the surface, and the triangle denotes the seismic station. (b) Travel time curves of four branches of PKP. Due to the unusual ray paths caused by scatterers in the lower mantle, the scattered waves can precede PKIKP by up to ~20 s. The shaded region indicates the possible earlier arrival times for precursors.

2. CMB region heterogeneities from PKP precursors

To constrain small-scale heterogeneities near the CMB beneath the Pacific region, we collected PKP precursor data recorded by Antarctic seismic arrays (GAMSIS and POLENET-ANET array) from earthquakes in the Aleutian Islands and Kamchatka Peninsula (Fig. 2). The GAMSEIS and POLENET/ANET networks consist of temporary and semi-permanent seismic stations deployed in East and West Antarctica beginning in 2008 for understanding the structure and solid-earth ice sheet interactions of the continent (Heeszel et al., 2013; Accardo et al., 2014; Anthony et al., 2015). These new seismic stations provide much improved coverage of the CMB along paths not previously sampled due to sparse global station distribution in the far-southern latitudes. Here we use 59 Antarctic seismic stations (26 in GAMSEIS and 33 in POLENET/ANET) deployed during 2009–2011, and earthquakes with magnitude greater than 5.5 (Table 1) at a distance range of 134–143°. All seismograms are band-pass filtered between 0.5 and 2.0 Hz, and only those with low noise levels and clear precursor signals are selected. PKP precursor travel times and envelope amplitudes are then analyzed to locate the scatterers and to calculate the velocity variations within them.

Fig. 3 shows representative PKP precursor waveforms from earthquakes in three different regions (western, middle and eastern region). The relative amplitudes of PKP precursors in the middle region (central panel) are obviously much larger than those in the other two regions, and are larger than the PKIKP phases at some distances. Investigating the larger sample of earthquakes in each region, we find that the amplitudes have no relation with the earthquake depth (Table 1). By comparing the entry and exit points of PKIKP rays at the CMB (Fig. 2) from these earthquakes, it is found that the exit points of the earthquakes from different regions are intermixed, while the entry points are well separated into different locations.

2.1. Results from PKP arrival times

To determine the exact locations of the seismic scatterers, we adopt Wen's method (Wen, 2000) that utilizes the arrival times of PKP precursors. First, we divide the region of the possible scatterer locations (20–50°N, 140–200°E, and from the CMB to 600 km above the CMB) into six depth ranges with separation of 100 km. In each depth range, the region is further divided into a 1.0° by 1.0° uniform grid of nodes. Then we calculate the scatterer probability and hit count for each node by comparing the predicted and observed precursor arrival times of all earthquakes. The probability at a given node is the ratio of the number of seismic rays whose PKP precursor onsets sample this node over the total number of seismic rays in this study, and the hit count is the number of PKP precursors sampling this node. Detailed information about the method can be found in Wen (2000). In general, the grids with high probability and large hit counts are most likely where the PKP precursors originate.

We calculate the hit counts and probability near the CMB region for both source side and receiver side. We find that, at the same depth, both the hit counts and probability for receiver side are smaller than those of the source side. Considering together the fact

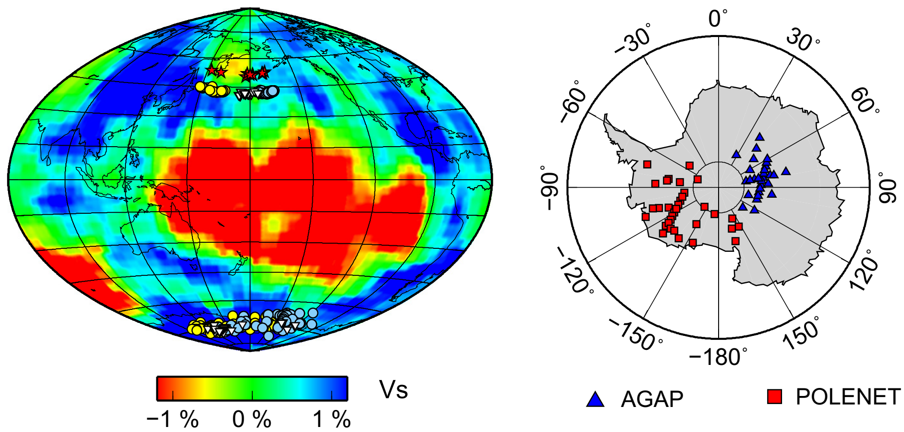

Fig. 2. Maps showing the distributions of the earthquakes and stations used in this study. (a) The background is the CMB shear velocity perturbation map from Grand (2002). The stars indicate earthquake locations. The circles with different colors and inverted triangles show PKIKP entry and exit points on the CMB generated by the three groups of earthquakes. Note that the earthquakes are divided into three groups (western, middle, and eastern region from left to right), and the entry points of the three groups of earthquakes at CMB are well separated on the source side while being intermixed on the receiver side. (b) Distributions of seismic stations in Antarctica. The squares and triangles denote GAMSEIS and POLENET/ANET network stations, respectively.

Table 1
Events used in this study for PKP precursor analysis.

Date	Time (GMT)	Latitude (deg)	Longitude (deg)	Depth (km)	Magnitude (mb)	Region
2009.01.26	19:11:47	51.9550	−171.1590	25.3000	5.6	East
2010.07.18	05:56:44	52.8760	−169.8480	14.0000	6.3	
2011.06.24	03:09:39	52.0500	−171.8360	52.0000	6.9	
2011.09.02	10:55:53	52.1710	−171.7080	32.0000	6.5	
2009.12.10	02:30:52	53.4170	152.7560	656.2000	6.1	West
2010.07.30	03:56:13	52.4980	159.8430	23.0000	6.1	
2009.03.30	12:07:28	51.5350	−178.2580	31.0000	6.0	Middle
2009.06.22	19:55:24	51.2770	−178.2010	35.0000	5.6	
2009.07.06	14:53:12	50.4350	176.9920	22.0000	6.0	
2009.10.07	05:38:37	52.1570	178.0520	138.4000	5.6	
2009.12.17	20:01:21	51.3980	179.9630	35.0000	6.2	

that the piercing points of PKIKP at the CMB are well separated in source side while are intermixed with each other in receiver side (Fig. 2), and the precursor waveform differences in different locations, we suggest that the precursors are most likely from the CMB region of the source side, the region to the north of the Pacific Anomaly.

Fig. 4 shows results of the scatterer probability and hit counts calculations for the three earthquake clusters at four depths in source side: the CMB, and 200 km, 300 km, 400 km above the CMB. The scattering regions are approximately distributed in 30–45°N in latitude, and 140–160°E, 160–180°E, 180–200°E in longitude, respectively (Fig. 4). Because the scatterer probability and hit counts in our study become insignificant at scattering depth shallower than 400 km above the CMB, we suggest that the scatterers are most likely confined within the lowermost 400 km of the mantle.

2.2. Results from PKP precursor amplitude

PKP precursor amplitude is determined not only by the scatterer location, but also their geometry, lateral distribution and velocity perturbation. Although PKP precursor arrival time can locate where the scatterers are, they cannot give any information about the velocity contrast between the scatterers and the ambient mantle. To solve this problem, we look further into the precursor amplitude.

We assume that the PKP precursors are due to PKP propagation through a random inhomogeneous elastic media. Based on Chernov's acoustic scattering theory (Chernov, 1960) adapted to elastic media (Haddon and Cleary, 1974; Doornbos, 1976), and assume the mantle behaves as a Poisson solid with single scattering and an exponential geostatistical autocorrelation function (Wu and Aki, 1985), the average scattered power can be written as (Hedlin et al., 1997; Hedlin and Shearer, 2000):

$$\langle|\Phi_s(\theta)|^2\rangle = \frac{2k^4a^3v^2VA^2}{\pi r^2}\frac{\frac{1}{4}\left[\cos(\theta)+\frac{1}{3}+\frac{2}{3}\cos^2(\theta)\right]^2}{\left[1+4k^2a^2\sin^2(\theta/2)\right]^2} \quad (1)$$

where V is the scattering volume, v the rms velocity perturbation, A is the incident wave amplitude, k is the wavenumber, r is the distance between the scatterer and receiver, and θ is the scattering angle.

We develop our own code to calculate the precursor energy based on Eq. (1). In our calculation, AK135 model (Kennett et al., 1995) is used, and both PKP AB and BC phase are considered for the precursor energy. We also include all the refraction coefficients and attenuation factors.

In this study, the scatterer volume can be calculated based on the results of Section 2.1. Previous studies have been empirically suggested that 6–10 km is the general scale length for scatterers within the Earth's lower mantle (e.g., Hedlin and Shearer, 2000; Helffrich and Wood, 2001; Mancinelli and Shearer, 2013). In order to compare with previous results, and because our observed pre-

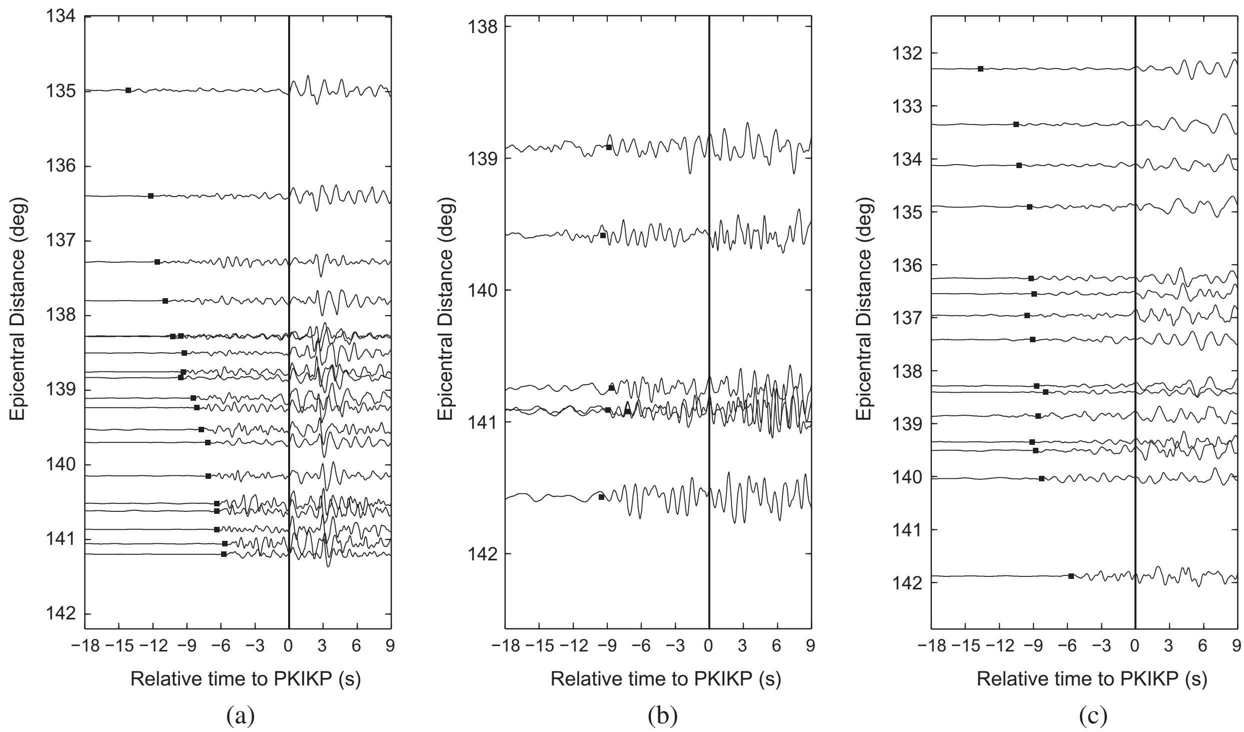

Fig. 3. Examples of PKP precursors observed in the Antarctic arrays from earthquakes in different locations (Fig. 2b). Each trace is aligned with the hand-picked PKIKP phase ($t = 0$). The hand-picked precursor onsets are marked by squares. The seismograms in (a) and (c) are from two events that occurred in western and eastern region, respectively. The seismograms in (b) are from events that occurred in the middle region. Note that the PKP precursors in (a) and (c) are weak while the precursors from the middle region show clear and comparable amplitudes to that of PKIKP waves.

cursors can only be seen at period less than 2 s, we choose 8 km as the scale length in our calculation. Using these assumptions, velocity perturbation is the only unknown and can be constrained by trial and error.

Similar to the method described in Section 2.1, we first divide the scattering volume into thinner (20 km) depth layers, with each layer further divided into $0.5^\circ \times 0.5^\circ$ grids. The area of each layer is based on the results from Section 2.1, so the scattering areas are different at different depths. Then for each grid node on each layer, we calculate its energy power based on Eq. (1). The energy kernel of each layer is obtained by summing up the scattering power of all the corresponding grid nodes in that layer.

Because the PKIKP phase in the seismogram may be contaminated by precursors, and it is difficult to obtain P waves with similar azimuths as PKIKP due to earthquake-station geometry, we could not extract the PKIKP source time function from observed seismograms. Instead, we use Direct Solution Methods (DSM; Geller and Takeuchi, 1995; Kawai et al., 2006) to calculate the synthetic seismograms for every station and then stack PKIKP phases to estimate the source time function for each event. In the calculation, all the attenuation and refraction coefficients are considered. The inner core attenuation is set to be 360 (Bhattacharyya et al., 1993). After convolving the energy kernels with the source time functions (in power), we calculate the square root of the energy power and normalize it to the theoretical amplitude of PKIKP.

Fig. 5 shows three representative seismograms from events located in the three different regions (west, middle and east). In this figure, the seismograms are binned over 1° distance and synthetic curves are superimposed on them. Note that the synthetic amplitudes increase gradually with distance and travel time. For the western and eastern regions (longitude 140–160°E, 180–200°E), the best fit is a model with ~0.5% bulk perturbation in P-wave velocity (Fig. 5a and c), and in the middle region (longitude 160–180°E), the best model is a scattering volume with 1.0–1.2% P-wave velocity perturbation (Fig. 5b). The amplitude variations of the scatterers in the three sub-regions suggest these regions must have different characteristics.

3. Results from S–ScS travel times

S-wave velocities can also be investigated to study the lower mantle characteristics near the scatterer locations. We searched the global data systematically for both broadband and long period tangential S waveforms. The earthquakes we selected are from 1990 to 2014. To obtain high-quality data, we only chose earthquakes with magnitude greater than 5.5 and depths greater than 100 km. The distance range of the S data is between 50° and 85° (Fig. 6).

After removing instrument response and transferring them to ground motion, we band-pass filtered the broad and long period data with frequency bands 0.05–2.0 Hz and 0.01–0.1 Hz, respectively. We carefully check the quality of those waveforms and finally select 423 waveforms.

ScS–S residual travel-times are defined as:

$$(\mathrm{ScS{-}S})_{\mathrm{residual}} = (\mathrm{ScS{-}S})_{\mathrm{observed}} - (\mathrm{ScS{-}S})_{\mathrm{predicted}} \tag{2}$$

Although differential travel times can reduce the error from uncertainties of earthquake location, origin time, and crust and upper mantle heterogeneities, it can be biased by heterogeneities from lower mantle (Wysession et al., 1994, 2001). We correct both S and ScS travel time anomalies above 400 km from the CMB using the 3-D tomographic model GypSuM (Simmons et al., 2010), thus reducing the heterogeneity effect from the mantle above our study region.

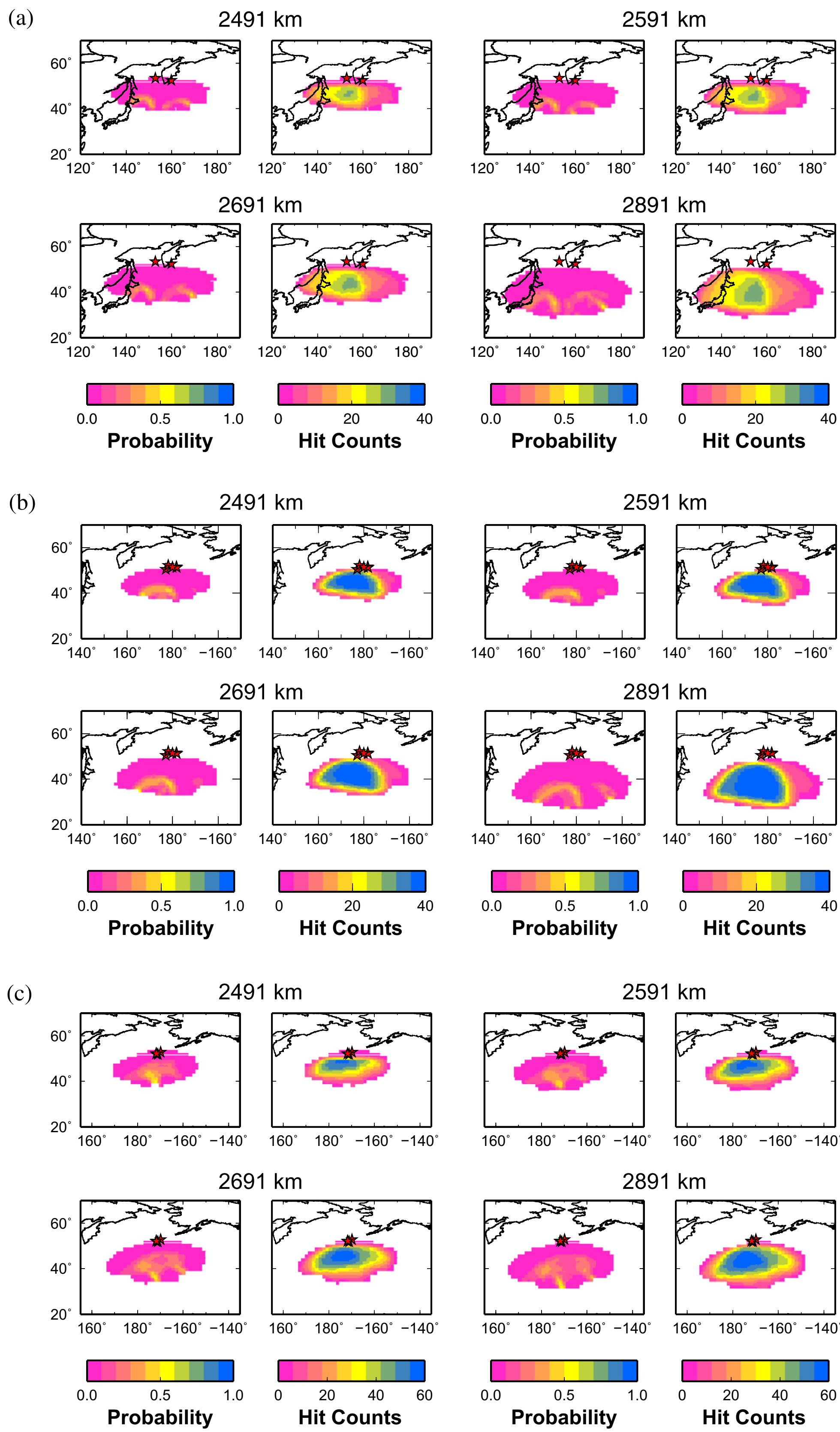

Fig. 4. Maps of scatterer probability and hit count for events in the western (a), middle (b), and eastern (c) region, respectively. Four depths of seismic scattering are presented: 0 km, 200 km, 300 km, and 400 km above the CMB. At each depth, the left figure is the scatterer probability map and the right is the hit count map. The red stars denote event locations. The regions with high scatterer probability and large hit count are considered to be the most likely locations from where the PKP precursor are generated.

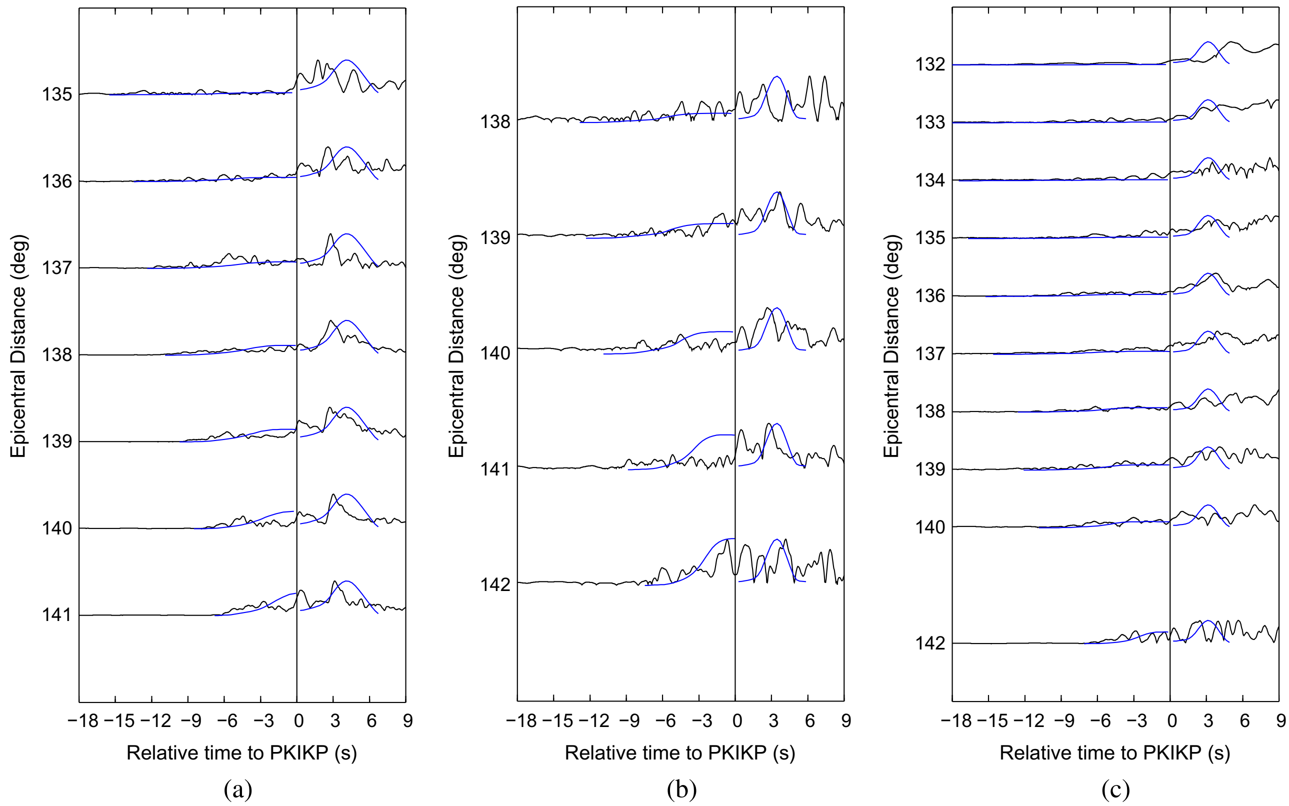

Fig. 5. Observed (black) and synthetic PKP precursor envelopes (blue) for three representative events in three regions (see Fig. 3). The seismograms are aligned with the hand-picked PKIKP phase ($t = 0$). The envelopes of PKIKP (black smoothed curve) for each event are stacked from individual seismograms, which are calculated using DSM (Kawai et al., 2006). (a and c) Synthetic curves are calculated for 0.5% rms velocity perturbation within 400 km above the CMB in the scattering regions shown in Fig. 4a and c. (b) Synthetic curves are the same as in (a and c) except for ∼1.2% velocity perturbation in the region in Fig. 4b. The scale length of the scatterers is 8 km in our model. (For interpretation of the references to color in this figure legend, the reader is referred to the web version of this article.)

Fig. 7 shows the relationship between S, ScS and ScS–S residuals. Obviously ScS residuals show strong correlation with ScS–S while S residuals show weak correlation. This relationship demonstrates that those differential ScS–S residuals are mainly from ScS path in the lowermost mantle, and negative residuals indicate the anomaly is from high-velocity heterogeneities.

We estimate S velocity variations based on the following equation

$$\delta v/v = -\delta t/t \tag{3}$$

where v is the averaged velocity, δt is the corrected travel-time residuals, and t is the total travel time of ScS through the bottom 400 km of the mantle.

Fig. 8 shows the distribution of averaged shear-velocity variations on ScS reflection points at the CMB. Although not all the scattering regions are well sampled, the three regions can still be distinguished and are sketched in the figure. The S-wave velocity variations are approximately 1.0–1.5% on the western and eastern regions, while the middle region shows a different S velocity variation of 2.0–3.0%.

A possible concern is that the travel times may be influenced by the adjacent Pacific Anomaly. Since most of the S waves travel well above the Pacific Anomaly, this is only a concern for the ScS phases. Thus we carefully checked the ScS piercing points at 400 km above the CMB, and found that all of them bypass the Pacific Anomaly's north boundary (Fig. 6). Therefore, the ScS travel time data are not affected by the Pacific Anomaly, and they show correct trend of the heterogeneities in the same region as the PKP precursors.

4. Discussion

4.1. Comparison with previous studies

There have been various studies on PKP precursors. In terms of global PKP precursor data, single scattering theory have proposed a model of 0.5% ± 0.1% rms velocity perturbations in a 200 km layer above the CMB (Bataille and Flatté, 1988), or 1.0% rms velocity perturbation in the whole mantle (Hedlin et al., 1997). On the other hand, multiple scattering theory has given different results. For example, Margerin and Nolet (2003b) suggested a model with 0.1% P velocity perturbations in the whole mantle, similar to the 0.2% whole mantle perturbation model proposed by Mancinelli and Shearer (2013). Margerin and Nolet (2003a) claimed that the single scattering theory could probably wrongly estimate the strength of the scatterer, and the limit of the rms velocity perturbation from single scatter would be 0.5%. Later, Mancinelli and Shearer (2013) found that the single and multiple scattering methods give similar results, and in all the scattered waves, single scattered waves dominate in number (90%).

Above studies are from averaged PKP precursors in global scale, so the PKP precursor amplitudes are weak. However, anomalous PKP precursors do exist in various regions, not only in amplitude, but also in shape (e.g., Vidale and Hedlin, 1998; Wen and Helmberger, 1998; Hedlin and Shearer, 2000; Vanacore et al., 2010; Waszek et al., 2015). These anomalies may reflect regional heterogeneities, such as in our study.

To further compare single and multiple scattering methods, we used the phonon code (Shearer and Earle, 2004; Mancinelli and Shearer, 2013), which considers all the scattered waves, to model

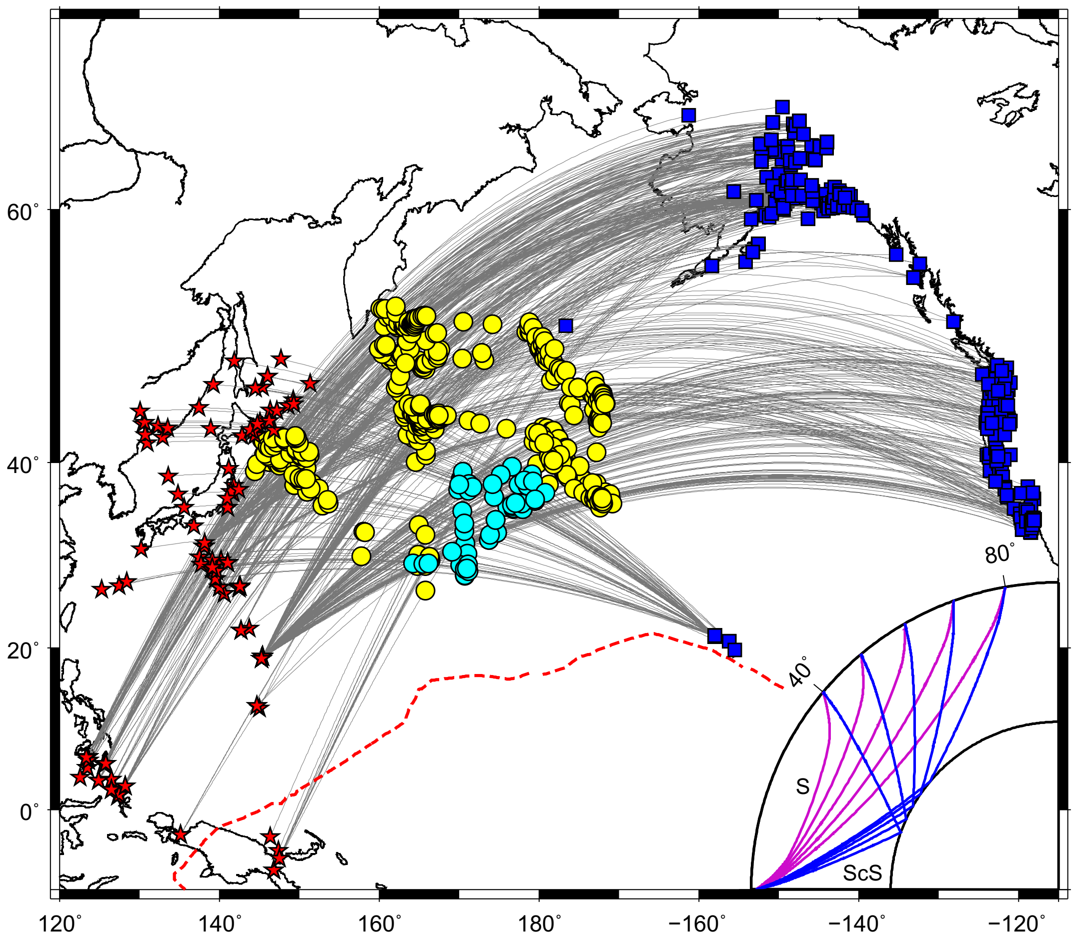

Fig. 6. Map of the study region with surface projection of ScS data. Yellow and cyan circles indicate ScS bouncing points at CMB from broadband and long-period data, respectively. The gray lines denote the great-circle path connecting the earthquakes (red stars) and seismic stations (blue squares). The red dashed line is the boundary of the Pacific Anomaly from He and Wen (2012). Note that the ScS paths bypass the Pacific Anomaly. The inset shows the ray paths of S and ScS at epicentral distances from 40° to 80°. Pink and blue lines denote the S and ScS ray-paths respectively. (For interpretation of the references to color in this figure legend, the reader is referred to the web version of this article.)

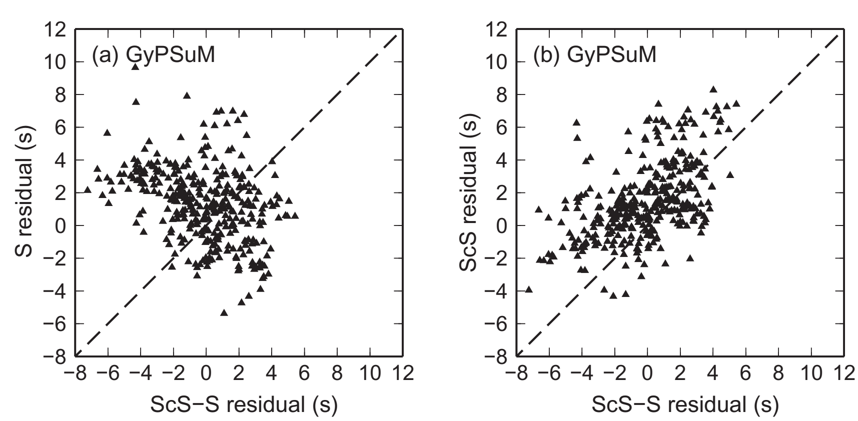

Fig. 7. Correlations between observed ScS–S residuals with S (a) and ScS (b) residuals after correcting travel time anomalies 400 km above the CMB using model GyPSuM10 (Simmons et al., 2010). Dashed lines are one to one correlation.

the precursor amplitudes of our data. We confine the scattering region in the 400 km above the CMB and set the scale length to 8 km, same as that in our single scattering modeling. The result suggests that P wave velocity perturbations of 0.2% and 0.5% on the two sides and the center region respectively fit the data well. Considering that we only confine depth in the multiple scattering modeling, the difference is understandable. We deduce that a more realistic regional scatterer should reduce the difference between these two methods. In general, the single and multiple scattering theory should produce similar results: on one hand, the single scat-

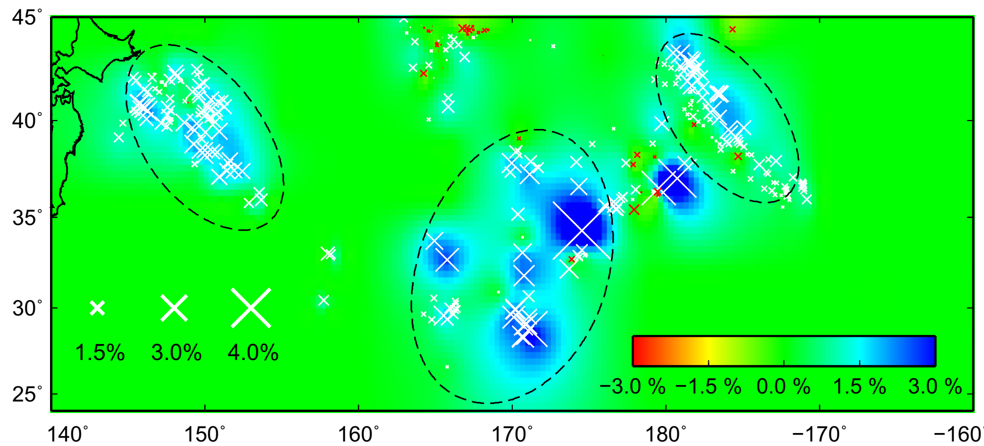

Fig. 8. Averaged shear wave velocity perturbations at the bottom 400 km of the lower mantle. The white crosses, which denote fast velocities, are plotted at ScS reflection points at the CMB. The background colors are smoothed S velocity perturbations based on our observations. Three regions (west, middle and east) with different heterogeneity variations are delineated approximately by the three dashed ellipses.

tered waves dominate the scattered waves in number; on the other hand, the intrinsic attenuation may suppress the multiple scattered waves more.

Finally, strong scattering in the lithosphere would also affect the precursor amplitude relative to the peak PKIKP (Mancinelli and Shearer, 2013), and neglecting this effect may overestimate the rms velocity perturbation of the scatterer. However, the lateral variations of the scattering strength would remain the same in our study. Because this effect is beyond the content of this paper, we did not investigate deeply on this topic.

4.2. Origin of the scatterers

Examination of mantle tomographic models (e.g., Grand, 2002; Zhao, 2004; Li et al., 2008; Simmons et al., 2010) shows that the heterogeneous regions identified in this study are part of the high-velocity anomalies near the CMB, as the ScS data have suggested. Although it has been long noticed that there is a "ring" of fast anomalies surrounding the slow anomalies in the center of Pacific (e.g., Wysession, 1996; Maruyama et al., 2007), the detailed structure and origin of these features still remain ambiguous.

Using P diffracted waves, Wysession (1996) inverted global large-scale heterogeneities near the CMB region, and found that northern Pacific rim region was coincident with the Panthalasa paleo-subduction. Based on geological and seismic tomographic data, Van der Meer et al. (2012) reconstructed intra-oceanic arc subduction and suggested that a series of paleo-subduction zones subducted in the mid-Panthalasa ocean. Their reconstruction results show that the locations of the subduction zones ~200 Myr ago overlap partly with the scatterer locations we find in the lowermost mantle. On the other hand, Maruyama et al. (2007) reconstructed the paleo-subduction location back to 180 Myr based on the hot spot frame and current plate movements. By comparing their results to the current tomographic structures in the mantle, they speculated that the high-velocity anomaly surrounding the Pacific Anomaly near the CMB was the graveyard of Rodinia subduction (0.75–1.0 Ga), since the high-velocity region does not correspond with the locations of Mesozoic subduction zones in their study.

Our results show that the fast regions to the north of the Pacific Anomaly have lateral variations, with central region having larger high velocity and two side regions having relatively smaller high velocities. Based on the previously described studies, we also suggest that the high velocity anomalies represent subducted paleo-slabs. A related question is how to interpret the different levels of velocity heterogeneity in the three sub-regions. One explanation is that the three sub-regions are from different paleo-slabs (Oku-Niikappu, Kolyma-Omolon, and Anadyr-Koryak plate, from left to right), and these slabs may have different thermal and subduction histories, as Van der Meer et al. (2012) have suggested.

Alternatively, these sub-regions could also be from a single paleo-slab, where different parts of the slab were separated during the segregation/mixing process of the slab in the CMB (Christensen and Hofmann, 1994). For example, Lee and Chen (2007) proposed that when the slab subducts into the mantle, the oceanic crust could separate from the underlying lithospheric mantle due to a weak serpentinized zone inside the slab. Because the oceanic crust transformed to high-pressure phases has negative buoyancy in the mantle, it can sink into the lower mantle (Stixrude and Lithgow-Bertelloni, 2012). Moreover, the rheological differences between the recycled crust and surrounding mantle may defer the homogenization and lead to incomplete mixing (Metcalfe et al., 1995; Helffrich and Wood, 2001; Van Keken et al., 2002), making it possible for the subducted slab to remain in the CMB region for a long time. Furthermore, during the homogenization, the segregation of different minerals within the crust could also result in compositional heterogeneities (Sun et al., 2011) because of low viscosity effects (here the Pacific Anomaly may serve this purpose). Thus, different compositions from a segregation process can explain our observed lateral variations within the fast anomalies.

The relative amplitude differences between PKP precursors and PKIKP are also affected by inner core attenuation (Wen and Niu, 2002; Waszek et al., 2015) or topography at the CMB (Doornbos, 1978; Bataille and Flatté, 1988). To test the inner core effect, we checked PKIKP turning points of the earthquakes in the three sub-regions, and found that they were highly random and intermixed with each other. Thus the regional inner core attenuation variations could not be the cause. We also chose different Q value from 250 to 600 (Cormier and Xu, 1998; Yu and Wen, 2006) in PKIKP synthetics, and found that the change of the relative amplitude is ~20%, which will not affect our result greatly. For topography effect, the largest PKP precursor amplitude in our study, similar to that of Wen (2000), would require topography of several kilometers at the CMB. According to Wen (2000), that is incompatible with CMB dynamics. Overall, we contend that the lower mantle heterogeneity model described here provides a good explanation for the PKP precursor observations and is consistent with ScS travel times and mantle tomographic models.

Although we have both P and S velocity variations in the study region, we did not compare them directly. The reason is that our P-wave velocity perturbations are statistical variations within a range, but S-wave velocity variations are absolute average variations in the region. Thus it is not proper to compare them directly. Investigation of the ratio of P and S anomalies would require similar observations and processing methods for both P and S waves.

5. Conclusions

We observe clear PKP precursors at Antarctica seismic stations from earthquakes in the Aleutian Islands and the Kamchacha Penisula. By analyzing the onsets and amplitudes of these precursors, we find that there exist seismic heterogeneities in the lowermost mantle to the north of Pacific Anomaly, between latitude 30–45°N. These heterogeneities exhibit lateral variations: the middle region (longitude 160–180°E) has small-scale P-wave velocity perturbations of 1.0–1.2%, while on the two sides (140–160°E and 180–200°E), the P-wave velocity perturbations are ~0.5%. Our ScS–S travel time residuals sampling similar regions also show similar results: the middle and the two sides have S velocity variations of about 2.0–3.0% and 1.0–1.5%, respectively.

The heterogeneities may be the remnants of ancient subducted slabs. We propose that the lateral variations are caused by either different slabs, or by different compositional fragments arising from material segregation during subduction.

Although there may be discrepancies between single and multiple scattering calculation in determining the rms perturbation of scatterer, our results suggest that they are generally on the same order. Other effects such as near surface scattering may need further investigation in the future.

Acknowledgments

We would like to thank V.F. Cormier and another reviewer for their constructive comments/suggestions, which have greatly improved the quality of the manuscript. We also thank N.J. Mancinelli and P.M. Shearer for providing us the phonon code generously. X. Ma and X. Sun are supported by China National Science Foundation (No. 41274057) and the 973 project of Ministry of Science and Technology of China (2014CB845901), and China National Science Foundation (No. 41330209). The Antarctic seismic data were collected with the support of the National Science Foundation of United States under grants ANT-0537597, ANT-0632209, and ANT-0838934. Figures are made using Generic Mapping Tools (Wessel and Smith, 1995). The facilities of IRIS Data Services, and specifically the IRIS Data Management Center, were used for access to waveforms, related metadata, and/or derived products used in this study. IRIS Data Services are funded through the Seismological Facilities for the Advancement of Geoscience and EarthScope (SAGE) Proposal of the National Science Foundation under Cooperative Agreement EAR-1261681. This is a contribution to No. IS-2188 of GIGCAS.

References

Accardo, N.J., Wiens, D.A., Hernandez, S., Aster, R.C., Nyblade, A., Huerta, A., Anandakrishnan, S., Wilson, T., Heeszel, D.S., Dalziel, I.W.D., 2014. Upper mantle seismic anisotropy beneath the West Antarctic Rift System and surrounding region from shear wave splitting analysis. Geophys. J. Int. 198, 414–429.
Anthony, R.E., Aster, R.C., Wiens, D.A., Nybalade, A., Anandakrishnan, S., Huerta, A., Winberry, J.P., Wilson, T., Rowe, C., 2015. The seismic noise environment of Antarctica. Seismol. Res. Lett. 86 (1), 89–100.
Bataille, K., Flatté, S.M., 1988. Inhomogeneities near the core–mantle boundary inferred from short-period scattered PKP waves recorded at the global digital seismograph network. J. Geophys. Res. 93 (B12), 15057–15064.
Bhattacharyya, J., Shearer, P., Master, G., 1993. Inner core attenuation from short-period PKP(BC) versus PKP(DF) waveforms. Geophys. J. Int. 114, 1–11.
Cao, A., Romanowicz, B., 2007. Locating scatterers in the mantle using array analysis of PKP precursors from an earthquake doublet. Earth Planet. Sci. Lett. 255, 22–31.
Chernov, L.A., 1960. Wave Propagation in a Random Medium R.A. Silverman, Trans.. McGraw-Hill, New York.
Christensen, U.R., Hofmann, W., 1994. Segregation of subducted oceanic crust in the convecting mantle. J. Geophys. Res. 99 (B10), 19867–19884.
Cleary, J.R., Haddon, R.A.W., 1972. Seismic wave scattering near the core–mantle boundary: a new interpretation of precursor to PKP. Nature 240, 549–551.
Cormier, V.F., 1995. Time-domain modelling of PKIKP precursors for constraints on the heterogeneity in the lowermost mantle. Geophys. J. Int. 121, 725–736.
Cormier, V.F., Xu, L., 1998. Seismic attenuation of the inner core: viscoelastic or stratigraphic? Geophys. Res. Lett. 25, 4019–4022.
Cormier, V.F., 1999. Anisotropy of heterogeneity scale lengths in the lower mantle from PKIKP precursors. Geophys. J. Int. 136, 373–384.
Doornbos, D.J., 1976. Characteristics of lower mantle inhomogeneities from scattered waves. Geophys. J. R. Astr. Soc. 44, 447–470.
Doornbos, D.J., 1978. On seismic-wave scattering by a rough core–mantle boundary. Geophys. J. R. Astr. Soc. 53, 643–662.
Frost, D.F., Rost, S., Selby, N.D., Stuart, G.W., 2013. Detection of a tall ridge at the core–mantle boundary from scattered PKP energy. Geophys. J. Int. 123, 449–470.
Garnero, E.J., Vidale, J.E., 1999. ScP: a probe of ultralow velocity zones at the base of the mantle. Geophys. Res. Lett. 26 (3), 377–380.
Garnero, E.J., 2000. Heterogeneity of lowermost mantle. Annu. Rev. Earth Planet. Sci. 28, 509–537.
Garnero, E.J., 2004. A new paradigm for Earth's core–mantle boundary. Science 304, 834–836.
Garnero, E.J., Maupin, V., Lay, T., Fouch, M.J., 2004. Variable azimuthal anisotropy in Earth's lowermost mantle. Science 306, 259–261.
Garnero, E.J., McNamara, A.K., 2008. Structure and dynamics of Earth's lower mantle. Science 320, 626–628.
Geller, R.J., Takeuchi, N., 1995. A new method for computing highly accurate DSM synthetic seismograms. Geophys. J. Int. 123, 449–470.
Grand, S.P., 2002. Mantle shear-wave tomography and the fate of subducted slabs. Philos. Trans. R. Soc. Lond. Ser. A 360, 2475–2491.
Haddon, R.A., Cleary, R.J., 1974. Evidence for scattering of seismic PKP waves near the core–mantle boundary. Phys. Earth Planet. Inter. 8, 211–234.
Hedlin, M.A.H., Shearer, P.M., 2000. An analysis of large-scale variations in small-scale mantle heterogeneity using Global Seismographic Network recordings of precursors to PKIKP. J. Geophys. Res. 105 (B6), 13665–13673.
Hedlin, M.A.H., Shearer, P.M., Earle, P.S., 1997. Seismic evidence for small-scale heterogeneity throughout the Earth's mantle. Nature 387, 145–150.
Heeszel, D.S., Wiens, D.A., Nyblade, A.A., Hansen, S.E., Kanao, M., An, M., Zhao, Y., 2013. Rayleigh wave constraints on the structure and tectonic history of the Gamburtsev Subglacial Mountains, East Antarctica. J. Geophys. Res. Solid Earth 118, 2138–2153.
He, Y., Wen, L., 2009. Structural features and shear-velocity structure of the "Pacific Anomaly". J. Geophys. Res. 114 B02309.
He, Y., Wen, L., 2012. Geographic boundary of the "Pacific Anomaly" and its geometry and transitional structure in the north. J. Geophys. Res. 117 B09308.
Helffrich, G., Wood, B., 2001. The Earth's mantle. Nature 412, 501–507.
Husebye, E.S., King, D.W., 1976. Precursors to PKIKP and seismic wave scattering near the mantle-core boundary. J. Geophys. Res. 81 (11), 1870–1882.
Kawai, K., Takeuchi, N., Geller, R.J., 2006. Complete synthetic seismograms up to 2 Hz for transversely isotropic spherically symmetric media. Geophys. J. Int. 164, 411–424.
Kendall, J.M., Silver, P.G., 1996. Constraints from seismic anisotropy on the nature of the lowermost mantle. Nature 381, 409–412.
Kennett, B.L.N., Engdahl, E.R., Buland, R., 1995. Constraints on seismic velocities in the Earth from travel times. Geophys. J. Int. 122, 108–124.
Lay, T., Williams, Q., Garnero, E.J., 1998. The core–mantle boundary layer and deep earth dynamics. Nature 392, 461–468.
Lay, T., Garnero, E.J., 2011. Deep mantle seismic modeling and imaging. Annu. Rev. Earth Planet. Sci. 39, 91–123.
Lee, C.-T.A., Chen, W., 2007. Possible density segregation of subducted oceanic lithosphere along a weak serpentinite layer and implications for compositional stratification of the Earth's mantle. Earth Planet. Sci. Lett. 255, 357–366.
Li, X., Romanowicz, B., 1996. Global mantle shear velocity model developed using nonlinear asymptotic coupling theory. J. Geophys. Res. 101 (B10), 22245–22272.
Li, C., van der Hilst, R.D., Engdahl, E.R., Burdick, S., 2008. A new global model for P wave speed variations in Earth's mantle. Geochem. Geophys. Geosyst. 9 Q05018.
Long, M.D., 2009. Complex anisotropy in D″ beneath the eastern Pacific from SKS–SKKS splitting discrepancies. Earth Planet. Sci. Lett. 283, 181–189.
Mancinelli, N.J., Shearer, P.M., 2013. Reconciling discrepancies among estimates of small-scale mantle heterogeneity from PKP precursors. Geophys. J. Int. 195, 1721–1729.
Margerin, L., Nolet, G., 2003a. Multiple scattering of high-frequency seismic waves in the deep earth: modeling and numerical examples. J. Geophys. Res. 108 (B5), 2234.
Margerin, L., Nolet, G., 2003b. Multiple scattering of high-frequency seismic waves in the deep Earth: PKP precursors analysis inversion for mantle granularity. J. Geophys. Res. 108 (B11), 2514.

Maruyama, S., Santosh, M., Zhao, D., 2007. Superplume, supercontinent, and post-perovskite: mantle dynamics and anti-plate tectonics on the core–mantle boundary. Gondwana Res. 11, 7–37.
McNamara, A.K., Zhong, S., 2005. Thermochemical structures beneath Africa and the Pacific Ocean. Nature 437, 1136–1139.
Metcalfe, G., Bina, C.R., Ottino, J.M., 1995. Kinematic considerations for mantle mixing. Geophys. Res. Lett. 22 (7), 743–746.
Miller, M.S., Niu, F., 2008. Bulldozing the core–mantle boundary: localized seismic scatterers beneath the Caribbean Sea. Phys. Earth Planet. Inter. 170, 89–94.
Ni, S., Helmberger, D.V., 2003. Seismological constraints on the South African superplume: could be the oldest distinct structure on earth. Earth Planet. Sci. Lett. 206, 119–131.
Niu, F., Wen, L., 2001. Strong seismic scatterers near the core–mantle boundary west of Mexico. Geophys. Res. Lett. 28 (18), 3557–3560.
Rost, S., Garnero, E.J., Williams, Q., 2006. Fine-scale ultralow-velocity zone structure from high-frequency seismic array data. J. Geophys. Res. 111 B09310.
Rost, S., Garnero, E.J., Stefan, W., 2010. Thin and intermittent ultralow-velocity zones. J. Geophys. Res. 115 B06312.
Shearer, P.M., Earle, P.S., 2004. The global short-period wavefield modelled with a Monte Carlo seismic phonon method. Geophys. J. Int. 158, 1103–1107.
Simmons, N.A., Forte, A.M., Boschi, L., Grand, S.P., 2010. GyPSuM: a joint tomographic model of mantle density and seismic wave speeds. J. Geophys. Res. 115 B12310.
Stixrude, L., Lithgow-Bertelloni, C., 2012. Geophysics of chemical heterogeneity in the mantle. Annu. Rev. Earth Planet. Sci. 40 (1), 569–595.
Sun, W., Ding, X., Hu, Y., Zartman, R.E., Arculus, R.J., Kamenetsky, V.S., Chen, M., 2011. The fate of subducted oceanic crust: a mineral segregation model. Int. Geol. Rev. 53 (8), 879–893.
Thomas, C., Kendall, J.M., Helffrich, G., 2009. Probing two low-velocity regions with PKP b-caustic amplitudes and scattering. Geophys. J. Int. 178, 503–512.
Thomas, C., Weber, M., Wicks, C.W., Scherbaum, F., 1999. Small scatterers in the lower mantle observed at German broadband arrays. J. Geophys. Res. 104 (B7), 15073–15088.
Vanacore, E., Niu, F., Ma, Y., 2010. Large angle reflection from a dipping structure recorded as a PKIKP precursor: evidence for a low velocity zone at the core–mantle boundary beneath the Gulf of Mexico. Earth Planet. Sci. Lett. 293, 54–62.
Van der Meer, D.G., Torsvik, T.H., Spakman, W., van Hinsbergen, D.J.J., Amaru, M.L., 2012. Intra-Panthalassa ocean subduction zones revealed by fossil arcs and mantle structure. Nat. Geosci. 5, 215–219.
Van Keken, P.E., Hauri, E.H., Ballentine, C.J., 2002. Mantle mixing: the generation, preservation, and destruction of chemical heterogeneity. Annu. Rev. Earth Planet. Sci. 30, 493–525.
Vidale, J.E., Hedlin, M.A.H., 1998. Evidence for partial melt at the core–mantle boundary north of Tonga from the strong scattering of seismic waves. Nature 391, 682–685.
Wang, Y., Wen, L., 2007. Geometry and P and S velocity structure of the "African Anomaly". J. Geophys. Res. 112 B05313.
Waszek, L., Thomas, C., Deuss, A., 2015. PKP precursor: implications for global scatterers. Geophys. Res. Lett. 42 (10), 3829–3838.
Wen, L., Helmberger, D., 1998. Ultra low velocity zones near the core–mantle boundary from broadband PKP precursors. Science 279, 1701–1703.
Wen, L., 2000. Intense seismic scattering near the core–mantle boundary beneath the Comoros hotspot. Geophys. Res. Lett. 27 (22), 3627–3630.
Wen, L., 2001. Seismic evidence for a rapidly varying compositional anomaly at the base of the Earth's mantle beneath the Indian Ocean. Earth Planet. Sci. Lett. 194, 83–95.
Wen, L., Niu, F., 2002. Seismic velocity and attenuation structures in the top of the Earth's inner core. J. Geophys. Res. 107 (B11), 2273.
Wessel, P., Smith, W.H.F., 1995. New version of the generic mapping tools released. EOS. Trans. Am. Geophys. Un. 76, 329.
Wysession, M.E., 1996. Large-scale structure at the core–mantle boundary from diffracted waves. Nature 382, 244–248.
Wysession, M.E., Bartkó, L., Wilson, J.B., 1994. Mapping the lowermost mantle using core–reflected shear waves. J. Geophys. Res. 99 (B7), 13667–13684.
Wysession, M.E., Fischer, K.M., Al-eqabi, G.I., Shore, P.J., Gurari, I., 2001. Using MOMA broadband array ScS–S data to image smaller-scale structures at the base of the mantle. Geophys. Res. Lett. 28 (5), 867–870.
Wu, R.S., Aki, K., 1985. Elastic wave scattering by a random medium and the small-scale inhomogeneities in the lithosphere. J. Geophys. Res. 90 (B12), 10261–10273.
Yao, J., Wen, L., 2014. Seismic structure and ultra-low velocity zones at the base of the Earth's mantle beneath Southeast Asia. Phys. Earth Planet. Inter. 233, 103–111.
Young, C.J., Thorne, L., 1987. The core–mantle boundary. Ann. Rev. Earth Planet. Sci. 15, 25–46.
Yu, W., Wen, L., 2006. Seismic velocity and attenuation structures in the top 400 km of the Earth's inner core along equatorial paths. J. Geophys. Res. 111 B07308.
Zhao, D., 2004. Global tomographic images of mantle plumes and subducting slabs: insight into deep Earth dynamics. Phys. Earth Planet. Inter. 146, 3–34.